Global Analysis of Protein Damage by the Lipid Electrophile 4-Hydroxy-2-nonenal*⃝S

Simona G. Codreanu‡, Bing Zhang§, Scott M. Sobecki¶, Dean D. Billheimer‖, and Daniel C. Liebler‡**

Lipid peroxidation yields a variety of electrophiles, which are thought to contribute to the molecular pathogenesis of diseases involving oxidative stress, yet little is known of the scope of protein damage caused by lipid electrophiles. We identified protein targets of the prototypical lipid electrophile 4-hydroxy-2-nonenal (HNE) in RKO cells treated with 50 or 100 μM HNE. HNE Michael adducts were biotinylated by reaction with biotinamidohexanoic acid hydrazide, captured with streptavidin, and the captured proteins were resolved by one dimensional sodium dodecyl sulfate-polyacrylamide gel electrophoresis, digested with trypsin, and identified by liquid chromatography-tandem mass spectrometry. Of the 1500+ proteins identified, 417 displayed a statistically significant increase in adduction with increasing HNE exposure concentration. We further identified 18 biotin hydrazide-modified, HNE-adducted peptides by specific capture using anti-biotin antibody and analysis by high resolution liquid chromatography-tandem mass spectrometry. A subset of the identified HNE targets were validated with a streptavidin capture and immunoblotting approach, which enabled detection of adducts at HNE exposures as low as 1 μM. Protein interaction network analysis indicated several subsystems impacted by endogenous electrophiles in oxidative stress, including the 26 S proteasomal and chaperonin containing TCP-1 (CCT) systems involved in protein-folding and degradation, as well as the COP9 signalosome, translation initiation complex, and a large network of ribonucleoproteins. Global analyses of protein lipid electrophile adducts provide a systems-level perspective on the mechanisms of diseases involving oxidative stress. *Molecular & Cellular Proteomics 8:670–680, 2009.*

The formation of oxidants is a hallmark of chemical toxicity, inflammation, and other types of environmental stresses (1, 2). Oxidative stress and oxidants are also involved in human diseases that account for significant morbidity and mortality, including cancer, atherosclerosis, and neurodegenerative diseases (3–8). Although oxidative stress derives fundamentally from the excessive flux of reduced oxygen species, such as superoxide, hydrogen peroxide, and hydroxyl radicals, secondary products of lipid, DNA, and protein oxidation may play critical roles in oxidant-associated molecular pathologies. Lipid peroxidation yields a variety of electrophilic, nonradical products, such as malondialdehyde, hydroxyalkenals, oxoalkenals, epoxyalkenals, and γ-ketoaldehydes (9, 10). These products are well known to form mutagenic DNA adducts, which are thought to contribute to oxidant-induced mutagenesis (11). However, reactive electrophiles also readily react with proteins. Protein modifications by malondialdehyde, 4-hydroxynonenal (HNE)[1] and 4-oxononenal have been characterized on a limited number of proteins by mass spectrometry (MS) (12–20) and in tissues by antibody-based methods (21–26). Although relatively little is known about the target selectivity of oxidant-derived lipid electrophiles in complex proteomes, a broader understanding of this phenomenon would provide a basis for understanding mechanisms of oxidant-induced stress and its role in many disease processes.

Recent work has demonstrated the application of activity-based probes combined with affinity capture of the target proteins and shotgun proteomics to identify functional components of complex proteomes (27, 28). In our previous work we have employed reactive biotin-tagged electrophiles and LC-MS-MS to perform global analyses of the cellular protein targets of reactive electrophiles (29–31). These studies have provided identification and sequence-specific mapping of over 1500 protein adducts. Global surveys of gene expression changes by cell stressors provide a means to assess the impact of DNA and protein damage at a systems level (32–35). This same general approach is applicable in principle to proteomics datasets (36) but has not yet been applied to datasets describing protein damage.

Here we describe the application of an adduct biotinylation and capture strategy combined with shotgun proteomic anal-

[1] The abbreviations used are: HNE, 4-hydroxynonenal; MS, mass spectrometry; LC-MS-MS, liquid chromatography-tandem mass spectrometry; HSP90, heat shock protein 90; GSTP, glutathione S-transferase P; GAPDH, glyceraldehyde-3-phosphate dehydrogenase; TrxRd1, thioredoxin reductase 1; Prdx6, peroxiredoxin 6; PBS, phosphate-buffered saline; MOPS, 4-morpholinepropanesulfonic acid; FDR, false discovery rate; LDS, lithium dodecyl sulfate.

ysis to perform global identification of HNE adducts in human cells. We employed biotin hydrazide, a reagent that reacts with the residual carbonyl moiety formed by the Michael addition of HNE to protein nucleophiles (37, 38). Because affinity capture methods in complex proteomes entail the potential for many false-positive identifications because of nonspecific binding, we used a label-free approach to quantify captured proteins as a function of HNE exposure concentration and then applied statistical analyses to identify protein targets demonstrating concentration-dependent adduction. In addition, we developed a generally applicable biotin capture and immunoblotting method to verify selected protein targets. This approach enables analysis of covalent adduction at the levels of systems and networks and provides a basis for understanding the functional impact of HNE adduction in cells.

MATERIALS AND METHODS

Materials—McCoy's 5A medium and fetal bovine serum were purchased from Invitrogen. HNE was obtained from Cayman Chemical (Ann Arbor, MI). Leupeptin, aprotinin, pepstatin, iodoacetamide, phenylmethylsulfonylfluoride, *N*-ethylmaleimide, sodium fluoride, sodium molybdate, sodium orthovanadate, β-glycerophosphate, and anti-biotin antibody-agarose were purchased from Sigma-Aldrich. Modified porcine sequencing grade trypsin was from Promega (Madison, WI). Streptavidin and AlexaFluor® 680-conjugated fluorescent secondary antibodies were obtained from Molecular Probes (Eugene, OR) and IRDye® 800-conjugated fluorescent secondary antibodies were obtained from Rockland Immunochemicals (Gilbertsville, PA). Anti-HNE-Michael reduced rabbit polyclonal antibody was purchased from EMD (San Diego, CA). Anti-heat shock protein 90 (HSP90) rabbit polyclonal antibody, anti-actin mouse monoclonal antibody, anti-tubulin rabbit polyclonal antibody, anti-cofilin rabbit polyclonal antibody, anti-glutathione *S*-transferase P (GSTP) rabbit polyclonal antibody, anti-glyceraldehyde-3-phosphate dehydrogenase (GAPDH) mouse monoclonal antibody, anti-thioredoxin reductase 1 (TrxRd1) mouse monoclonal antibody, and anti-peroxiredoxin 6 (Prdx6) rabbit polyclonal antibody were purchased from Abcam (Cambridge, MA). Anti-cullin3 goat polyclonal antibody and anti-bax rabbit polyclonal antibody were purchased from Santa Cruz (Santa Cruz, CA). All other chemical reagents were purchased from commercial sources and were used without further purification. All solutions were prepared fresh before each use.

Cell Culture and in Vivo HNE Treatment—RKO human colorectal carcinoma cells used in this study were grown in McCoy's 5A medium supplemented with 10% fetal bovine serum, at 37 °C in an atmosphere of 95% air/5% CO_2. Treatments were carried out with varying concentrations of HNE dissolved in ethanol. Confluent cells plated in 150-mm culture dishes were washed with cold phosphate-buffered saline and incubated with 0, 50, or 100 μM HNE delivered in 10-ml McCoy's 5A medium without fetal bovine serum. The total concentration of ethanol per culture was ≤0.1% of the total medium volume. Cells were exposed to electrophile for 1 h at 37 °C in an atmosphere of 95% air/5% CO_2, then scraped off the culture dishes, centrifuged at 100 $\times$ *g* for 5 min, and washed two times with cold phosphate-buffered saline, pH 7.4. Cell pellets were lysed on ice in 2 ml of cold M-PER buffer (Pierce, Rockford, IL) supplemented with 150 mM NaCl, protease inhibitor mixture (1.0 mM phenylmethylsulfonylfluoride, 1.0 mM *N*-ethylmaleimide, 10 μg ml^{-1} leupeptin, 10 μg ml^{-1} aprotinin, 10 μg ml^{-1} pepstatin), and phosphatase inhibitor mixture (1.0 mM sodium fluoride, 1.0 mM sodium molybdate, 1.0 mM sodium orthovanadate, 10.0 mM β-glycerophosphate) for each plate. The lysate was

cleared by centrifugation at 10,000 $\times$ *g* for 10 min to remove cellular debris, and the total protein concentration of the supernatant was determined using BCA protein assay (Pierce).

Immunoblot Analysis of Electrophile-treated RKO Cells—To detect HNE modification of RKO cell proteins by HNE *in vivo*, lysates from treated cells (prepared as described above) were reduced with sodium borohydride, 100 mM final concentration, for 1 h at room temperature to stabilize the Michael adduct formed by HNE molecule with cysteine, lysine, or histidine residues on present proteins. Aliquots of the reduced lysates containing HNE-adducted proteins were then resolved by 10% SDS-PAGE using NuPAGE Bis-Tris gels (Invitrogen). The proteins were electrophoretically transferred to a polyvinylidene difluoride membrane (Invitrogen) and probed with anti-HNE-Michael reduced rabbit polyclonal antibody. AlexaFluor® 680-labeled goat anti-rabbit secondary antibody was used to detect HNE-adducted proteins. Immunoreactive proteins were visualized using the Odyssey™ Infrared IYmaging System and Odyssey software as described by the manufacturer (Li-Cor, Lincoln, NE).

Derivatization of HNE-adducted Proteins—Biotinylation of the carbonyl group in HNE-adducted proteins was achieved with biotin hydrazide (Fig. 1). Protein concentration of the lysates from treated cells (prepared as described above) was reduced to 2 mg/ml by addition of lysis buffer. Biotin hydrazide was added to a final concentration of 5 mM, and the mixture was incubated with gentle rotation at room temperature for 2 h in the dark. Hydrazone bonds were reduced with addition of sodium borohydride to a final concentration of 100 mM, followed by incubation for an additional 60 min at room temperature. Excess reagents were removed by filtration using 10,000 molecular weight cutoff Amicon Ultra concentrators (Millipore, Bedford, MA), and the buffer was exchanged to PBS, pH 7.4.

Streptavidin Affinity Capture of HNE-adducted Proteins—Biotinylated proteins resuspended in lysis buffer were incubated with streptavidin-agarose beads (~2 mg protein per 1-ml bead slurry previously equilibrated with lysis buffer) for 2 h with rotation at room temperature. The bound proteins were washed two times with 1% SDS solution in PBS, two times with 4 M urea solution in PBS, two times with 1 M NaCl solution in PBS, and two times with 1×PBS, pH 7.4, each first time wash with each of the reagents rotating the beads for 30 min at room temperature. After each wash step, the beads were centrifuged at 10,000 $\times$ *g* for 1 min, and the supernatant was discarded. The bound proteins were released from the beads by eluting the beads in LDS electrophoresis buffer at 95 °C for 15 min. Aliquots of the protein eluates (20 μl) were then subjected to immunoblot analyses. Both derivatized proteins from treated cells loaded on the beads and adducted proteins purified by streptavidin capture as described above were resolved by 10% SDS-PAGE using NuPAGE Bis-Tris gels. The proteins were electrophoretically transferred to a polyvinylidene difluoride membrane and probed with streptavidin. Immunoreactive proteins were visualized using the Odyssey® Infrared Imaging System and Odyssey software as described by the manufacturer (Li-Cor, Lincoln, NE).

In-gel Digestion of Adducted Proteins—Adducted proteins purified by streptavidin capture as described above were resolved by 10% SDS-PAGE using NuPAGE Bis-Tris gels and stained with Colloidal Coomassie Blue (Invitrogen). Bands corresponding to different molecular weights (17 fractions for each individual HNE treatment) were excised from the gel and digested in-gel with trypsin (39). Each excised band was chopped into 1-mm cubes and placed in 0.5-ml Eppendorf tubes containing 100 μl of 100 mM ammonium bicarbonate, pH 8.0. Samples were reduced with 10 μl of 45 mM dithiothreitol for 20 min at 55 °C and alkylated with 10 μl of 100 mM iodoacetamide for 20 min at room temperature in the dark. Samples were destained with 100 μl of 50% acetonitrile and 50 mM ammonium bicarbonate. The gel pieces were then dehydrated with 100% acetonitrile and

digested with trypsin (50 μl of 0.01 μg/μl Trypsin Gold (Promega) in 25 mM ammonium bicarbonate) overnight at 37 °C. The peptides were extracted with two rounds of 60% acetonitrile and 0.1% trifluoroacetic acid. They were dried down and reconstituted in 0.1% formic acid.

Anti-biotin Affinity Capture of HNE-adducted Peptides—Proteins from an untreated control and a 100 μM HNE-treated sample, following the derivatization and filtration steps, were resuspended in 100-μl 4×LDS electrophoresis buffer containing 50 μM dithiothreitol, boiled for 10 min at 70 °C, and loaded on a 10% NuPAGE Bis-Tris 2-well gel using the MOPS buffer system and antioxidant (500 μl antioxidant/ 200 ml MOPS). Proteins were electrophoresed ~2 cm into the gel, then the gel was removed, and proteins were fixed, followed by staining and destaining. The entire Coomassie-stained protein band was excised and chopped into 1-mm cubes and placed in 1.5-ml Eppendorf tubes containing 100 mM ammonium bicarbonate. Proteins were digested in-gel as described above, and peptides were extracted with two rounds of 60% acetonitrile and 0.1% trifluoroacetic acid. The peptide solution was evaporated *in vacuo* and reconstituted in 1 ml of buffer containing 50 mM MOPS, pH 7.2, 10 mM sodium phosphate, and 50 mM NaCl. The peptide solutions were transferred into the microfuge tubes containing 400 μl of the anti-biotin antibody agarose (Sigma-Aldrich) bead/buffer slurry (50:50 v:v) and were incubated with gentle rotation at 4 °C overnight. The beads were centrifuged at 1500 × g for 1 min, and the supernatant was removed. The beads were washed three times with 1 ml of buffer, then three times with 1 ml of water by inverting the tubes 5 times, centrifuging at 1500 × g for 1 min, and the supernatant was discarded. The adducted peptides were eluted by adding 100 μl of 0.15% trifluoroacetic acid to the beads with gentle agitation for 10 min. The beads were centrifuged at 1500 × g for 1 min, and the supernatant (containing biotin-HNE-adducted peptides) was transferred another microfuge tube. This step was repeated twice, and the combined supernatant was evaporated *in vacuo* and reconstituted in 50 μl of 0.1% formic acid.

LC-MS-MS Analyses—The resulting peptides were subjected to LC-MS-MS analysis using a ThermoFinnigan LTQ ion trap mass spectrometer equipped with a Thermo MicroAS autosampler and Thermo Surveyor high pressure liquid chromatography pump, Nanospray source, and Xcalibur 1.4 instrument control. Peptides were resolved on 100 μm × 11 cm-fused silica capillary column (Polymicro Technologies, LLC Phoenix, AZ) packed with 5 μm, 300 Å Jupiter C18 (Phenomenex, Torrance, CA) over 30 min with a 2% to 35% acetonitrile/H$_2$O linear gradient, where both mobile phases (solvents A and B) contained 0.1% (v/v) formic acid. Liquid chromatography was carried out at ambient temperature at a flow rate of 0.6 μl/min. Centroided MS-MS scans were acquired using an isolation width of 2 m/z, an activation time of 30 ms, an activation Q of 0.250, and 30% normalized collision energy using 1 microscan with a maximum ion time of 100 ms for each MS-MS scan. The mass spectrometer was tuned prior to analysis using the synthetic peptide TpepK (AVAGKAGAR) so that some parameters may have varied slightly from experiment to experiment, but typically the tune parameters were as follows: spray voltage of 2 kV, a capillary temperature of 150 °C, a capillary voltage of 50 V, and tube lens of 120 V. The MS-MS spectra of the peptides were collected using data-dependent scanning in which one full MS spectrum was followed by four MS-MS spectra. MS-MS spectra were recorded using dynamic exclusion of previously analyzed precursors for 60 s.

Biotin hydrazide-derivatized, HNE-adducted peptides captured with anti-biotin as described above were subjected to LC-MS-MS analysis using a ThermoFinnigan LTQ-Orbitrap hybrid mass spectrometer (Thermo Electron, San Jose, CA) equipped with an Eksigent nanoLC and autosampler (Dublin, CA). Peptides were resolved on a 100-μm × 11 cm-fused silica capillary column (Polymicro Technologies LLC, Phoenix, AZ) packed with 5 μm, 300 Å Jupiter C18 (Phe-

nomenex, Torrance, CA). Liquid chromatography was carried out at ambient temperature at a flow rate of 0.6 μl min^{-1} using a gradient mixture of 0.1% (v/v) formic acid in water (solvent A) and 0.1% (v/v) formic acid in acetonitrile (solvent B). Centroided MS-MS scans were acquired on the LTQ-Orbitrap using an isolation width of 2 m/z, an activation time of 30 ms, an activation Q of 0.250, and 35% normalized collision energy using 1 microscan with a maximum ion time of 100 ms for each MS-MS scan and 1 microscan with a max ion time of 1000 ms for each full MS scan. The mass spectrometer was tuned prior to analysis using the synthetic peptide TpepK (AVAGKAGAR), so that some parameters may have varied slightly from experiment to experiment, but typically the tune parameters were as follows: spray voltage of 2 KV, a capillary temperature of 150 °C, a capillary voltage of 50 V, and tube lens of 120 V. The AGC target value was set at 1,000,000 for the full MS and 10,000 for the MS/MS spectra. A full scan was obtained for eluting peptides in the range of 400–2000 amu and was collected on the Orbitrap portion of the instrument at a resolution of 60,000, followed by five data-dependent MS-MS scans on the LTQ portion of the instrument with a minimum threshold of 1000 set to trigger the MS/MS spectra. MS-MS spectra were recorded using dynamic exclusion of previously analyzed precursors for 60 s with a repeat of 1 and a repeat duration of 1s.

Peptide and Protein Identification and Identification of HNE-adducted Peptides—The "ScanSifter" algorithm v0.1, an in-house developed software, read tandem mass spectra stored as centroided peak lists from Thermo RAW files and transcoded them to DTA files. Spectra that contained fewer than 6 peaks or that had less than 2e1 measured TIC did not result in DTAs. If 90% of the intensity of a tandem mass spectrum appeared at a lower m/z than the precursor ion, a single precursor charge was assumed; otherwise, the spectrum was processed under both double and triple precursor charge assumptions. Proteins were identified using the SEQUEST v.27 (rev.12) algorithm (40) on a high speed, multiprocessor Linux cluster in the Advanced Computing Center for Research & Education at Vanderbilt University using the human subset of the International Protein Index (IPI) human protein database, version 3.31 created 7/20/07. To estimate false discovery rates, each sequence of the data base was reversed and concatenated to the data base, for a total of 135,168 entries. The data base search encompassed tryptic peptides with a maximum of 5 missed cleavage sites for enzyme search and with a maximum number of 10 internal cleavage sites. All cysteines were expected to undergo carboxamidomethylation and were assigned a mass of 160 kDa. All methionines were allowed to be oxidized. Precursor ions were required to fall within 1.25 m/z of the position expected from their average masses, and fragment ions were required to fall within 0.5 m/z of their monoisotopic positions. The database searches produced raw identifications in SQT file format (spectral data SEQUEST search results) (41).

Peptide identification, filtering, and protein assembly were done with IDPicker software (42). Initial filtering took place in multiple stages. First, IDPicker filtered raw peptide identifications to a target false discovery rate (FDR) of 5%. The peptide filtering employed reversed sequence data base match information to determine thresholds that yielded an estimated 5% FDR for the identifications of each charge state by the formula FDR = $(2R)/(R + F)$, where R is the number of passing reversed peptide identifications, and F is the number of passing forward (normal orientation) peptide identifications. The second round of filtering removed proteins supported by less than two distinct peptide identifications in the analyses. Indistinguishable proteins were recognized and grouped. Parsimony rules were applied to generate a minimal list of proteins that explained all of the peptides that passed our entry criteria (42).

The identification of biotin hydrazide-modified, HNE-adducted peptides was undertaken through a multistage analysis of MS-MS

spectra from anti-biotin capture of the biotinylated, adducted peptides. Peptides with modifications corresponding to HNE plus biotin hydrazide (511.6 Da) were identified with the SEQUEST v.27 (rev.12) algorithm as described above, allowing for variable modifications at Cys, His, and Lys residues. The data base searches produced raw identifications in SQT format (41). Peptide identification, filtering, and protein assembly were done with IDPicker software (42). Peptide filtration took place in multiple stages. First, IDPicker filtered raw peptide identifications to a target FDR of 10%. The second round of filtration allowed for proteins supported by only one distinct HNE-modified peptide identification in the analyses. Indistinguishable proteins were recognized and grouped. Parsimony rules were applied to generate a minimal list of proteins that explained all of the peptides that passed our entry criteria (42). Only those peptides and proteins respectively were considered HNE-adducted which appeared only in the treated sample and were not present in the control sample. All adducts were required to have measured precursor m/z values within 5 ppm of calculated values. Finally, all putative adducted peptide spectra were subjected to visual inspection to confirm assignment of major fragment ions, the continuity of b- and y-ion fragment series and neutral losses of water from the adducts or serine or threonine residues.

Statistical Analysis—Linear regression was used to evaluate the effect of HNE concentration on protein expression as quantified by the square root of spectral counts. Fit separately for each protein, this model allows a different intercept for each experiment, yet assumes a common slope per protein. A 10% FDR (43) was used to judge proteins responding to increasing HNE concentration. The 10% FDR balances a sensitive selection procedure for including affected proteins while limiting the expected number of false inclusions.

After accounting for replicate and HNE concentration effects, spectral count variability can be described by the Poisson distribution. The Poisson has the characteristic that the variance is equal to the mean. The square root transformation is known to stabilize the Poisson variance (44) so that it is approximately constant across mean values. The linear regression model used in the analysis of the spectral counts assumes that the variance is constant across changing mean levels.

Functional Classification and Network Analysis—HNE-adducted proteins identified in the regression analysis were classified and evaluated for functional category enrichment based on the Gene Ontology annotation using WebGestalt (45). In the enrichment analysis, all genes in the human genome were used as a background, and the enrichment p values calculated using the Hypergeometric test were adjusted for multiple tests (45). HNE-adducted proteins were also mapped to a human protein interaction network built locally by integrating data collected from HPRD, MINT, intact, REACTOME, and DIP. Only manually curated interactions were considered to assure the reliability of the network. A subnetwork comprising only the HNE-adducted proteins were further constructed. Clustering coefficient was calculated according to Watts and Strogatz (46). Network randomization was performed following Maslov and Sneppen (47). Protein communities in the subnetwork were identified using CFinder (48), and visualized using Cytoscape (49).

Protein Target Validation—Presence of HNE-adducted proteins from the RKO-treated cells was confirmed by probing with a fluorescently labeled streptavidin probe to determine overall biotinylation after derivatization with biotin hydrazide in either whole cell lysates or streptavidin-enriched samples. To validate specific protein targets adducted by HNE and identified by the overall LC-MS-MS analysis, RKO cells were incubated with 0, 50, or 100 μM HNE, and cell extracts were derivatized with biotin hydrazide and applied to streptavidin bead columns as described previously. Both the flow-through and elution fractions were collected and subjected to immunoblot analysis

with antibodies directed against proteins that had been detected by LC-MS-MS as putative HNE targets. Proteins that were adducted by HNE were detected by Western blotting in the elution fractions, which contained adducted proteins. Blots were probed for HSP90, actin, β-tubulin, cofilin, glutathione-S transferase P (GSTP), GAPDH, TrxRd1, Prdx6, cullin3, and bax.

RESULTS

Global Analysis of Protein Adduction by Lipid Oxidation-derived Model Electrophile HNE—To evaluate protein targets of lipid oxidation-derived electrophiles, we employed HNE, the most widely studied electrophile product of lipid peroxidation, which reacts with protein nucleophiles to form both Michael adducts (via 1,4-addition) and Schiff base adducts (via 1,2-addition). Although the latter reaction occurs with lysine ε-amines, the formation of Michael adducts is the dominant pathway for adduction of cysteine thiols, histidine imidazoles, and lysine ε-amines (50). Michael addition of HNE to these targets forms adducts with a residual carbonyl group, which is available for reaction with biotin hydrazide (38). We employed the human colon carcinoma RKO cell line for these studies based on related work in this system that evaluated the induction of electrophile covalent binding, gene expression changes, and toxicity by HNE (51–53).

The relatively low stoichiometry of protein adduction by electrophiles under relevant conditions necessitates an affinity enrichment approach because of the large excess of unmodified proteins in HNE-treated cells. The major complication of affinity enrichment approaches for shotgun proteomics is the artifactual capture of proteins through nonspecific interaction with affinity purification medium. The use of an untreated control is an unsatisfactory solution because many nonspecifically bound proteins are inevitably detected, particularly abundant proteins or those with structural features that interact with the support (agarose beads). Such proteins may be real targets of HNE, but would be eliminated from consideration because of their appearance in the control samples. We addressed this problem by exposing cells to increasing concentrations of HNE (50 and 100 μM), which generated concentration-dependent increases in protein adducts because of the pseudo-first order kinetic relationships that governed HNE adduction to proteins (54). The levels of adduction were compared on the basis of spectral counts for detected peptides (*i.e.* the number of MS-MS spectra acquired for a peptide is proportional to its concentration in the sample) (55). We also performed replicate experiments for the untreated controls and both HNE exposure concentrations to enable the incorporation of measurement variability into the statistical analysis. This approach is summarized in Fig. 1.

To determine optimal exposure concentrations, RKO cells were incubated with HNE at concentrations between 0 and 100 μM for one hour, and the adducted proteins were biotinylated by reaction with biotin hydrazide; the biotin tags were stabilized by reduction of the hydrazones with sodium borohydride, and the biotinylated proteins were captured with
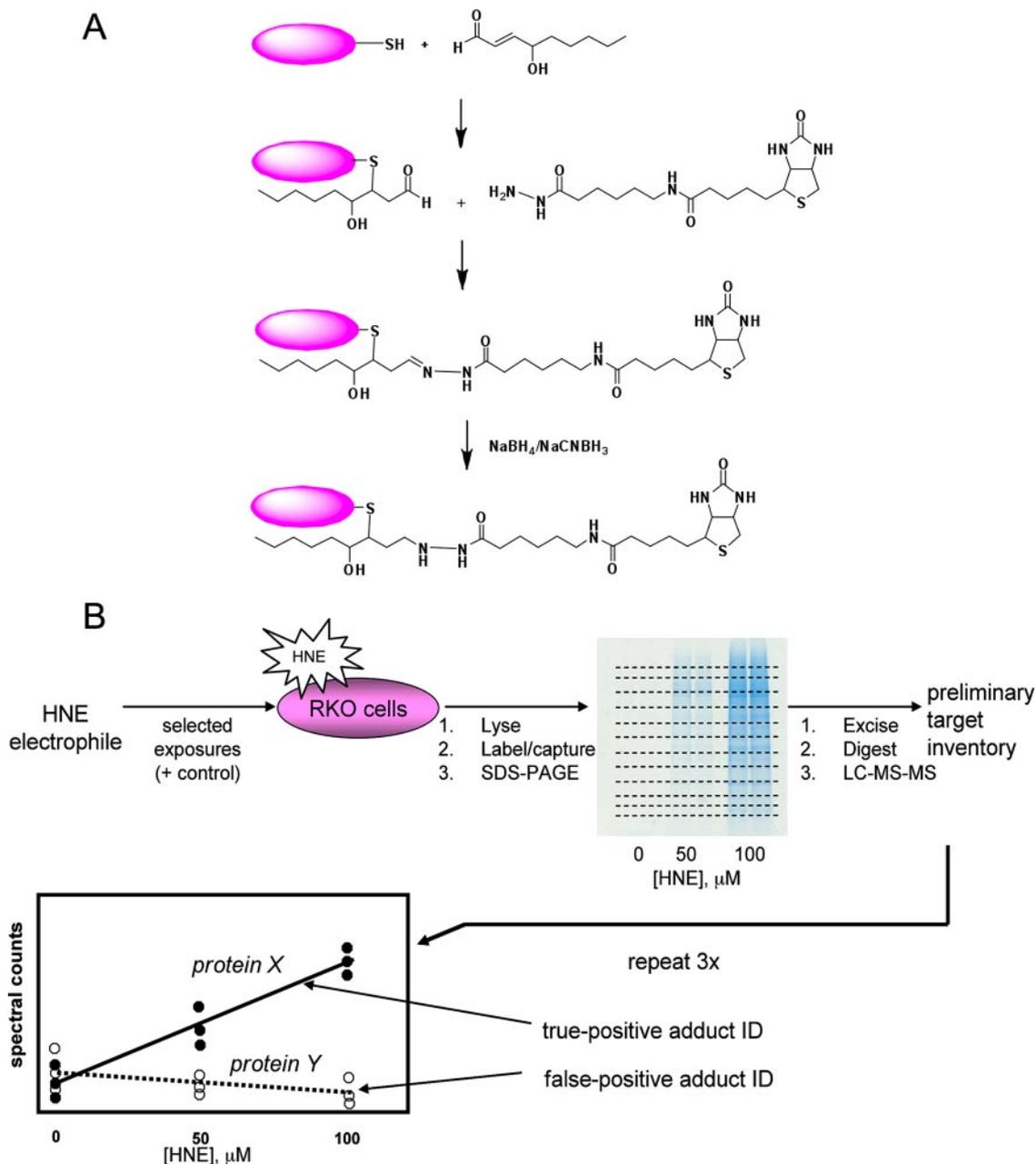
FIG. 1. *A*, biotinylation of protein reactive carbonyls with biotin hydrazide. *B*, experimental flow chart for identification of protein targets of HNE in RKO cells.

streptavidin. Western blotting with the anti-HNE antibody and streptavidin (supplemental Fig. S1) revealed that *in vivo* treatment with the electrophile produced a concentration-dependent increase in adduct formation across the entire proteome, with the most significant degree of adduction detected at 50 and 100 μM HNE concentrations. Time-dependent treatment of RKO cells with HNE revealed that one-hour incubation with the electrophile showed the highest degree of adduction by anti-HNE antibody and streptavidin (supplemental Fig. S1).

Identification of HNE-adducted Proteins by Biotinylation and LC-MS-MS—HNE-adducted proteins were biotinylated by reaction with biotin hydrazide and captured with streptavidin following stabilization of the captured adducts with sodium borohydride. Samples from vehicle control-treated dimethyl sulfoxide (DMSO) cells were processed in the same manner. Three replicate experiments were done for each HNE concentration and DMSO control, and each replicate experiment was analyzed once. Biotinylated proteins were captured on streptavidin-agarose, and after extensive washing to remove most non-biotinylated proteins, the biotinylated proteins were released by boiling in SDS-PAGE loading buffer and then resolved by SDS-PAGE. Each gel lane was cut into
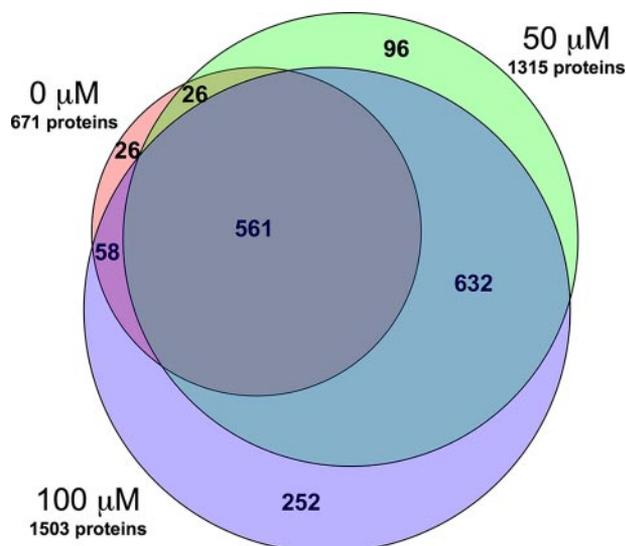
FIG. 2. **Overlap of adducted proteins identified from RKO cells treated with 50 or 100 μM HNE or vehicle control.** The numbers represent total proteins identified in triplicate analyses of each experimental condition. Overlaps between treatments are indicated by the numbers in the corresponding segments. A total of 561 proteins were common to all groups.

17 fractions, which were then subjected to in-gel tryptic digestion, and the resulting peptides were analyzed by LC-MS-MS on a ThermoFinnigan LTQ ion trap instrument. Peptides identified by data base searching at 95% confidence were assembled to generate parsimonious protein lists (42). Visual inspection of the Coomassie-stained SDS-PAGE gels indicated a strong concentration dependence of overall protein recovery on HNE treatment concentration with no detectable staining in controls (supplemental Fig. S2). However, LC-MS-MS analyses indicated that totals of 671, 1315, and 1503 discernible proteins were identified for the untreated control, the 50 μM and 100 μM HNE-treated samples, respectively (Fig. 2). Although the numbers of identified proteins increased with HNE treatment concentration, the high numbers of proteins identified in the untreated controls underscored the need to correct for nonspecific protein capture or possibly the presence of endogenous, biotin hydrazide-reactive carbonyls in proteins from untreated cells. As noted above, proteins that are true HNE targets are expected to display an electrophile concentration-dependent relationship, in which spectral counts for adducted proteins increase with HNE concentration. Linear regression was used to evaluate the effect of HNE concentration on protein adduction using a square root transformation for spectral count data. To accommodate variation in replicate experiments, a replicate effect was included in the statistical model. Fit separately for each protein, this model allows a different intercept for each experiment, yet assumes a common slope per protein (Fig. 1). A 10% FDR (43) was used to select 417 proteins responding to increasing HNE concentration. Effects for replicate and HNE concentration were included in the statistical (linear regression) model, but no other normalization was used.

A complete listing of the 417 HNE-adducted proteins is provided in supplemental Table S1. The HNE target proteins were classified based on the Gene Ontology annotation using WebGestalt and mapped to a broad range of biological processes, molecular functions, and cellular locations. A substantial proportion of these were intracellular proteins involved in metabolic processes. As metabolic proteins are often highly abundant, a key question is whether HNE reacts with specificity or simply targets high abundant proteins with little specificity. To address this question, we performed the same streptavidin capture and LC-MS-MS analysis on samples from untreated cell lysates. A Coomassie-stained SDS-PAGE gel used to resolve streptavidin-captured proteins following treatment of RKO cells with either no treatment or 100 μM HNE revealed no difference in protein patterns for untreated or HNE-treated RKO cellular lysate, yet indicated significant difference in banding patterns between untreated cellular lysates and protein pull-downs by streptavidin after biotinylation (supplemental Fig. S5). As shown in supplemental Table S2, of the 30 proteins with the highest spectral counts in the 100 μM HNE-treated samples, only half were identified in the untreated cell lysates. Similarly, of the 30 proteins with the highest spectral counts in the untreated cell lysates, 6 were not identified in the 100 μM HNE-treated samples. The overall correlation between the two samples as measured by the Spearman's correlation coefficient (rank correlation) between corresponding spectral counts was 0.044, which indicates a poor degree of correlation. These results clearly demonstrate that HNE does not simply react with proteins on the basis of their abundance, but instead displays specificity in reaction with protein targets.

To address whether HNE protein damage manifests selectivity for specific cell components and processes, we evaluated the enrichment of the HNE-adducted proteins in various Gene Ontology categories using all genes in the human genome as a background (supplemental Fig. S3). Categories enriched with HNE-adducted proteins included the *biological processes* "cell cycle" (35 proteins, FDR 0.002), "cellular component organization and biogenesis" (85 proteins, FDR 1.33e-7), "primary metabolic process" (239 proteins, FDR 5.79e-11), and "protein transport" (30 proteins, FDR 0.001); the *molecular functions* "antioxidant activity" (6 proteins, FDR 0.001), "translation regulator activity" (18 proteins, FDR 4.53e-9), and "structural molecule activity" (30 proteins, FDR 0.007); and the *cellular components* "cytoskeleton" (58 proteins, FDR 3.66e-10), and "mitochondrion" (47 proteins, FDR 5.60e-8).

Networks and Communities of HNE-adducted Proteins—To gain a systems-level understanding of the potential impact of HNE adduction, we built a human protein interaction network based on protein interaction data collected from various public data bases and mapped the HNE-adducted proteins to the network. A subnetwork of HNE-adducted proteins was further constructed to investigate the organization of these proteins using clustering coefficient analysis. The clustering coefficient

FIG. 3. **Protein communities identified from the network of HNE-adducted proteins.**
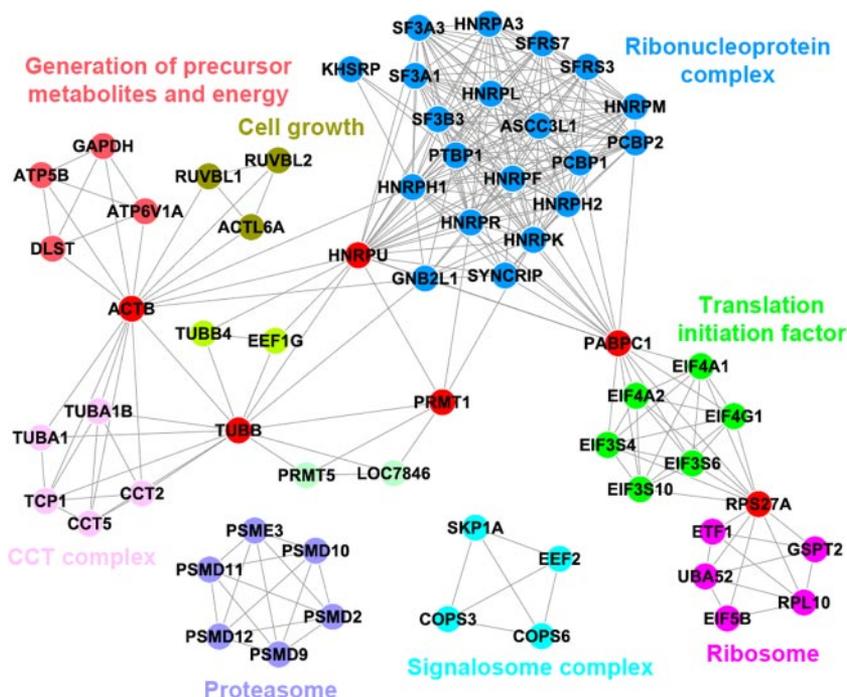
of a network characterizes the overall tendency of nodes to form clusters or communities (46). The subnetwork of HNE-targeted proteins had a clustering coefficient of 0.14, which was significantly higher than the average clustering coefficient of 0.027 obtained from 1,000 random subnetworks generated by randomly sampling the same number of proteins from the full human protein interaction network ($p < 2.2e-16$). This result could indicate that HNE might frequently target multiple proteins of a community coordinately, possibly because of common biochemical characteristics shared by the components in a community (*e.g.* common protein domains shared by proteins in the same complex). However, as the average number of interaction partners for the HNE-adducted proteins was 26.59, which is much higher than the average number of 13.86 for all proteins, the high clustering coefficient could also be explained by the higher node degrees observed for the HNE-adducted proteins. To test whether this is the case, we generated 1,000 randomized versions of the full human protein interaction network through a switching algorithm (47) and built one subnetwork of HNE-adducted proteins for each of these randomized networks. Although these randomized networks had exactly the same degree distribution as the real network, corresponding subnetworks of HNE-adducted proteins showed an average clustering coefficient of 0.016, which was significantly lower than that of the real subnetwork ($p < 2.2e-16$). This result suggests that the high clustering coefficient could not simply be explained by the high node degrees.

As HNE tends to coordinately target multiple proteins of a community, we used the software CFinder to explore the community structure in the network of HNE-targeted proteins. Fig. 3 depicts the network of protein communities identified

by this analysis. Protein communities targeted by HNE included ribonucleoprotein complexes, translation initiation factors, proteasome, CCT complex, and COP signalosome complex.

Validation of HNE-adducted Proteins by Biotinylation and Anti-biotin Peptide Capture—We performed additional studies to directly map adducts on some of the HNE-adducted proteins from an untreated control and a 100 μM HNE-treated sample. The protein mixture was subjected to the derivatization and filtration steps and then loaded onto a two-well gel using the MOPS buffer system. Proteins were resolved about 2 cm into the gel and then the gel was subjected to in-gel tryptic digestion. The resulting peptides were captured on anti-biotin antibody-agarose beads and, after extensive washing to remove non-biotinylated peptides, the biotinylated (HNE-adducted) peptides were released from the beads with 0.15% trifluoroacetic acid. Samples from an untreated control sample were processed in the same manner. The captured peptides were subjected to LC-MS-MS analysis using a Thermo LTQ-Orbitrap hybrid mass spectrometer. These analyses indicated a total number of 18 discernible HNE-adducted peptides that appeared only in the treated sample and were not present in the control sample. A complete listing of the HNE-adducted peptides and proteins, respectively, is provided in supplemental Table S3. Of the 18 adducted proteins identified by the peptide capture experiment, 14 correspond to the intact proteins captured (see above). Full scan MS and an MS-MS spectra for each of these 18 adducted peptides are included in supplemental Figs. S7–S19.

Sensitive Detection of Adduction of Specific Proteins by Biotin-avidin Capture and Immunoblotting—The identities of

some of the protein targets discovered by the LC-MS-MS analyses were validated by targeted measurements of the protein adducts using a combined biotin-avidin capture and immunoblotting approach. RKO cells were treated with HNE and then the adducted proteins were derivatized by reaction with biotin hydrazide and captured with streptavidin as described above. Both the flow-through and elution fractions were collected and subjected to immunoblot analysis with antibodies directed against proteins that had been detected by LC-MS-MS as putative HNE targets. Biotinylated proteins were eluted from the streptavidin beads by boiling them in

FIG. 4. **Immunoblotting validation of ten individual protein targets from RKO cellular extracts treated with increasing concentrations of HNE.** The presence of the proteins was confirmed in the input (*I*), flow-through (*F*), and elution (*E*) fractions (*arrows*), which contained adducted proteins.

LDS loading buffer. Blots were probed for HSP90, actin, tubulin, cofilin, GSTP, GAPDH, TrxRd1, Prdx6, cullin3, and bax. Treatment of RKO cells with 0, 50, 100 μM HNE was used to generate RKO protein adducts as for the LC-MS-MS-based studies described above. Examination of these blots clearly shows differences in protein adduction between 0, 50, and 100 μM HNE treatment (Fig. 4). Proteins adducted by HNE were detected by immunoblotting in the elution (*E*) fractions (Fig. 4, denoted by *arrows*), which contained adducted proteins. Immunoblot band intensities for the eluted fractions increased with HNE concentrations, and the changes in immunoblot intensity matched changes in adduction observed by spectral counting in LC-MS-MS (Fig. 5). We note that although this approach clearly indicates protein adduction changes, it may be possible to improve the quantitative precision of the assay by incorporating a fixed amount of some biotinylated protein (*e.g.* albumin) as an internal standard.

Together, both approaches identified and confirmed the presence of HNE-adducted proteins from RKO-treated cells. However, the concentrations of HNE employed in LC-MS-MS adduct identification studies (50 and 100 μM) may exceed levels expected under physiologic or pathophysiologic conditions. To validate some of the identified proteins as HNE targets at lower HNE concentrations, we again employed the biotinylation, streptavidin capture, and immunoblotting approach described above. Treatment of cells with 1, 5, 10, and 50 μM HNE revealed dose-dependent adduct formation as indicated by total biotinylated proteins (Fig. 6*A*) and by streptavidin capture and immunoblotting for actin, tubulin, HSP90, GSTP, and cul3 (Fig. 6*B*). Nevertheless, biotin hydrazide clearly labeled proteins in untreated RKO cells (Fig. 6*B*). This may indicate either nonspecific streptavidin-protein binding in both immunoblots and in streptavidin captures despite the extensive washing in the latter (see under "Materials and Methods"), reaction of biotin hydrazide with acceptor moieties
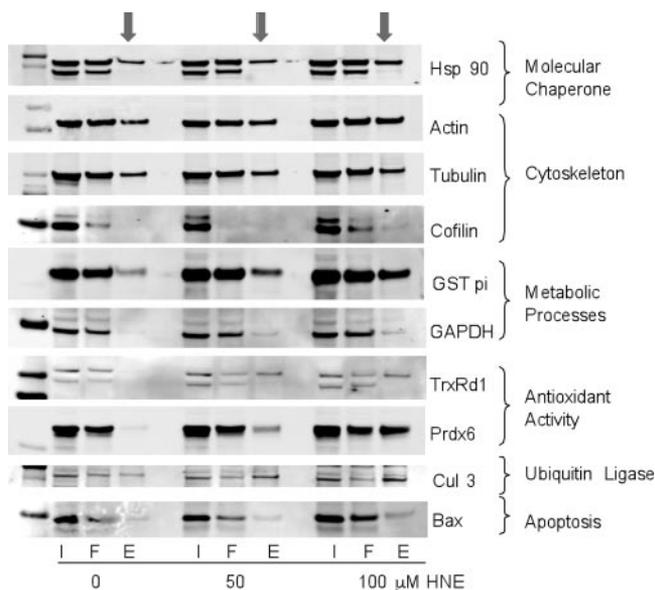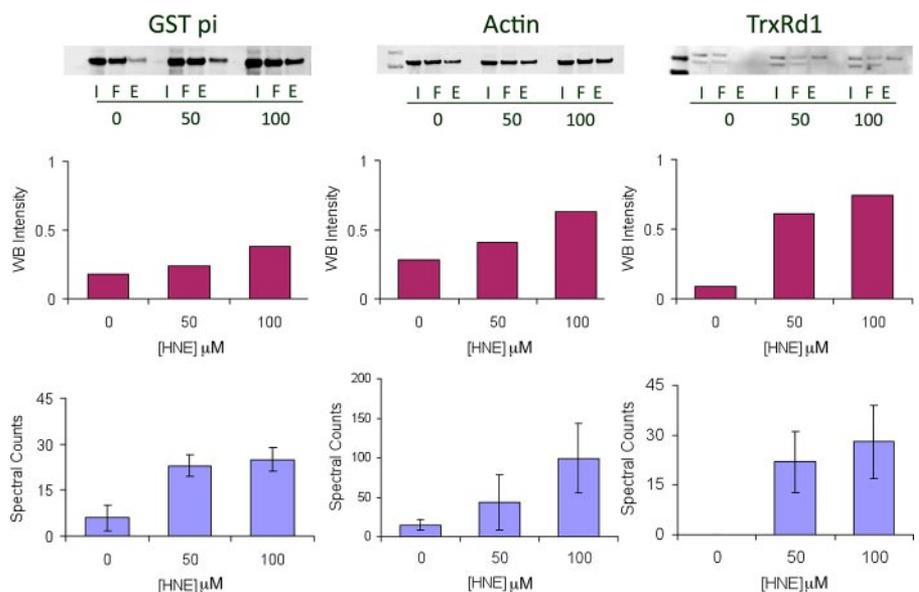
FIG. 5. **Semiquantitative analysis of three protein targets, GSTP, actin, and TrxRd1, based on spectral counts (*blue*) and immunoblot band intensity (*purple*).** Spectral count plots depict mean ± S. D.

FIG. 6. **Detection of biotinylated proteins from RKO cells treated with 0, 1, 5, 10, and 50 μM HNE and then derivatized with biotin hydrazide.** *A*, streptavidin immunoblot of total RKO cell protein extract with increasing protein labeling with HNE exposure concentration. *B*, immunoblot detection of the indicated proteins following RKO cell treatment with HNE, biotin hydrazide derivatization, capture of biotinylated proteins on streptavidin beads, and elution as described under "Materials and Methods."
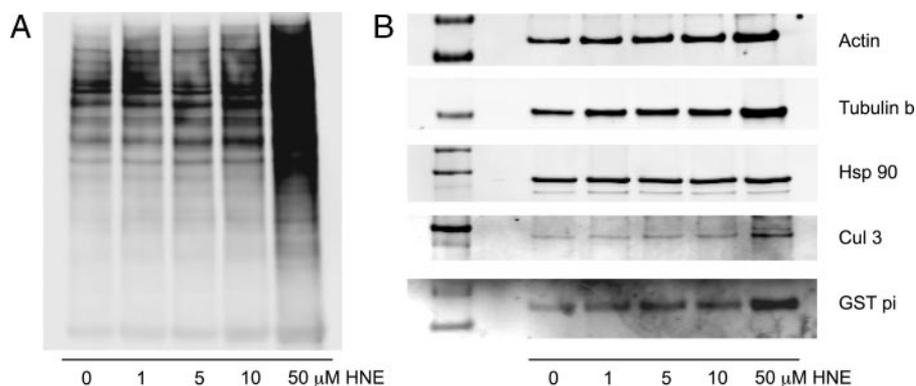
other than carbonyls, or the presence of endogenous protein carbonyls in untreated cells. All of these possibilities seem somewhat plausible, and none can be excluded. We also note that in Fig. 6*A*, it is evident that several distinct protein bands are biotin hydrazide-labeled in untreated controls and that these bands increase prominently with increasing HNE exposure. This observation could be explained by the presence of endogenous carbonyl-containing adducts on proteins that have high reactivity toward both endogenous electrophiles and HNE.

DISCUSSION

This work represents the most extensive global survey of protein damage by a lipid electrophile and provides useful example of both the potential and challenges of this approach. Selective analysis of protein adducts requires an affinity capture method. Here we employed biotin hydrazide to label HNE adducts, but other approaches employing affinity postlabeling via Click chemistry or similar methods are certainly applicable (28, 51, 56). Although affinity capture enriches for adducted proteins, nonspecific binding of proteins to affinity-capture medium results in false positive target identifications. We employed a statistical analysis of the concentration-dependence of protein adduct identification to circumvent this problem. Moreover, we validated several of HNE targets with an affinity capture and immunoblot strategy that is generally applicable to determining whether any protein of interest is a target of modification, provided that an antibody is available. As with the LC-MS-MS analyses, establishing a concentration-dependence for protein modification is used to minimize artifactual misidentification of protein targets. We also validated 35 modified peptides by specific capture of the adducted peptides using anti-biotin affinity capture and analysis by high resolution LC-MS-MS.

The exposure concentrations of HNE used in our studies (50–100 μM) are ~2–10-fold higher than HNE levels required to produce adaptive responses or apoptosis (52). Our preliminary experiments and other recent work (51) indicated that shotgun proteomic analysis of RKO cells exposed to lower HNE concentrations yielded far fewer protein target identifications. Use of higher HNE concentrations enabled detection

of greater numbers of adducts, but the relative distributions of adducts should be largely independent of HNE concentration in the concentration range of our experiments. This assumption is based on our previous work showing that HNE adduction of individual sites on albumin displays pseudo first-order kinetics in the micromolar-millimolar range (54). Thus, use of higher HNE concentrations enables discovery of adduct targets by LC-MS-MS. We should also note that the relative distribution of protein labeling by exogenous addition of HNE may be somewhat different from when HNE is generated endogenously during oxidative stress. Our application of the streptavidin capture and immunoblotting approach enabled confirmation of protein targets identified by LC-MS-MS, even at low HNE levels (Fig. 6).

Analysis of the protein targets of HNE in the context of functional networks provides a systems-level view of the potential impact of protein damage. HNE adduct targets were significantly represented in several functional systems or networks (Fig. 3). These included the 26 S proteasome system, which is responsible for the regulated degradation of many intracellular proteins and is essential for cell survival. Previous work indicates that proteasome function can be inhibited by oxidants and oxidative stress (57, 58). Two recent reports indicate that HNE adduction to proteasome subunits inhibits specific catalytic functions and impairs the degradation of protein substrates (59, 60). Because some adducted proteins are prone to misfolding and formation of aggregates (61), the dual effects of lipid electrophiles - protein adduction leading to misfolding and inhibition of proteasomal activity - are thought to contribute to neurodegenerative disease processes (62).

Related to this theme of protein damage and quality control is the appearance of members of the CCT complex as HNE targets. This chaperonin complex consists of two identical stacked rings, each containing eight different proteins (63). The complex folds various proteins, including actin, tubulin, and WD-40 repeat proteins, which all have been identified as targets for electrophile adduction (29).

Although the examples above illustrate the concordance between HNE adduction of functional protein complexes or subproteomes and known manifestations of protein damage,

our analyses also suggest that HNE and other lipid electrophiles may impact other functional systems, such as the COP9 signalosome complex, translation initiation complex, and a large network of ribonucleoproteins that manage the processing and transport of RNA. Interrogation of these systems in models of oxidative stress may advance understanding of how protein damage contributes to mechanisms of dysregulation, toxicity, and disease associated with oxidative stress.

REFERENCES

1. Ames, B. N. (1983) Dietary carcinogens and anticarcinogens. Oxygen radicals and degenerative diseases. *Science* **221,** 1256–1264
2. Halliwell, B. (1994) Free radicals, antioxidants, and human disease: curiosity, cause, or consequence? *Lancet* **344,** 721–724
3. Butterfield, D. A. (2002) Amyloid beta-peptide (1–42)-induced oxidative stress and neurotoxicity: implications for neurodegeneration in Alzheimer's disease brain. A review. *Free Radic. Res.* **36,** 1307–1313
4. Perry, G., Nunomura, A., Hirai, K., Zhu, X., Perez, M., Avila, J., Castellani, R. J., Atwood, C. S., Aliev, G., Sayre, L. M., Takeda, A., and Smith, M. A. (2002) Is oxidative damage the fundamental pathogenic mechanism of Alzheimer's and other neurodegenerative diseases? *Free Radic. Biol. Med.* **33,** 1475–1479
5. Beckman, K. B., and Ames, B. N. (1998) The free radical theory of aging matures. *Physiol. Rev.* **78,** 547–581
6. Ames, B. N. (2001) DNA damage from micronutrient deficiencies is likely to be a major cause of cancer. *Mutat. Res.* **475,** 7–20
7. Mashima, R., Witting, P. K., and Stocker, R. (2001) Oxidants and antioxidants in atherosclerosis. *Curr. Opin. Lipidol.* **12,** 411–418
8. Cai, H., and Harrison, D. G. (2000) Endothelial dysfunction in cardiovascular diseases: the role of oxidant stress. *Circ. Res.* **87,** 840–844
9. Porter, N. A., Caldwell, S. E., and Mills, K. A. (1995) Mechanisms of free radical oxidation of unsaturated lipids. *Lipids* **30,** 277–290
10. Roberts, L. J., Salomon, R. G., Morrow, J. D., and Brame, C. J. (1999) New developments in the isoprostane pathway: identification of novel highly reactive gamma-ketoaldehydes (isolevuglandins) and characterization of their protein adducts. *FASEB J.* **13,** 1157–1168
11. Marnett, L. J., and Plastaras, J. P. (2001) Endogenous DNA damage and mutation. *Trends Genet.* **17,** 214–221
12. Liu, Z., Minkler, P. E., and Sayre, L. M. (2003) Mass spectroscopic characterization of protein modification by 4-hydroxy-2-(E)-nonenal and 4-oxo-2-(E)-nonenal. *Chem. Res. Toxicol.* **16,** 901–911
13. Bolgar, M. S., Yang, C. Y., and Gaskell, S. J. (1996) First direct evidence for lipid/protein conjugation in oxidized human low density lipoprotein. *J. Biol. Chem.* **271,** 27999–28001
14. Alderton, A. L., Faustman, C., Liebler, D. C., and Hill, D. W. (2003) Induction of redox instability of bovine myoglobin by adduction with 4-hydroxy-2-nonenal. *Biochemistry* **42,** 4398–4405
15. Lin, D., Lee, H. G., Liu, Q., Perry, G., Smith, M. A., and Sayre, L. M. (2005) 4-Oxo-2-nonenal is both more neurotoxic and more protein reactive than 4-hydroxy-2-nonenal. *Chem. Res. Toxicol.* **18,** 1219–1231
16. Zhu, X., and Sayre, L. M. (2007) Long-lived 4-oxo-2-enal-derived apparent lysine Michael adducts are actually the isomeric 4-ketoamides. *Chem. Res. Toxicol.* **20,** 165–170
17. Carbone, D. L., Doorn, J. A., Kiebler, Z., Sampey, B. P., and Petersen, D. R. (2004) Inhibition of Hsp72-mediated protein refolding by 4-hydroxy-2-nonenal. *Chem. Res. Toxicol.* **17,** 1459–1467
18. Carbone, D. L., Doorn, J. A., Kiebler, Z., and Petersen, D. R. (2005) Cysteine modification by lipid peroxidation products inhibits protein disulfide isomerase. *Chem. Res. Toxicol.* **18,** 1324–1331
19. Carbone, D. L., Doorn, J. A., Kiebler, Z., Ickes, B. R., and Petersen, D. R. (2005) Modification of heat shock protein 90 by 4-hydroxynonenal in a rat model of chronic alcoholic liver disease. *J. Pharmacol. Exp. Ther.* **315,** 8–15
20. Sampey, B. P., Carbone, D. L., Doorn, J. A., Drechsel, D. A., and Petersen, D. R. (2007) 4-Hydroxy-2-nonenal adduction of extracellular signal-regulated kinase (Erk) and the inhibition of hepatocyte Erk-Est-like protein-1-activating protein-1 signal transduction. *Mol. Pharmacol.* **71,** 871–883
21. Li, C. J., Nanji, A. A., Siakotos, A. N., and Lin, R. C. (1997) Acetaldehyde-modified and 4-hydroxynonenal-modified proteins in the livers of rats with alcoholic liver disease. *Hepatology* **26,** 650–657
22. Uchida, K., Sakai, K., Itakura, K., Osawa, T., and Toyokuni, S. (1997) Protein modification by lipid peroxidation products: formation of malondialdehyde-derived N(epsilon)-(2-propenol)lysine in proteins. *Arch. Biochem. Biophys.* **346,** 45–52
23. Montine, K. S., Kim, P. J., Olson, S. J., Markesbery, W. R., and Montine, T. J. (1997) 4-hydroxy-2-nonenal pyrrole adducts in human neurodegenerative disease. *J. Neuropathol. Exp. Neurol.* **56,** 866–871
24. Hartley, D. P., Kolaja, K. L., Reichard, J., and Petersen, D. R. (1999) 4-Hydroxynonenal and malondialdehyde hepatic protein adducts in rats treated with carbon tetrachloride: immunochemical detection and lobular localization. *Toxicol. Appl. Pharmacol.* **161,** 23–33
25. Yoritaka, A., Hattori, N., Uchida, K., Tanaka, M., Stadtman, E. R., and Mizuno, Y. (1996) Immunohistochemical detection of 4-hydroxynonenal protein adducts in Parkinson disease. *Proc. Natl. Acad. Sci. U. S. A.* **93,** 2696–2701
26. Uchida, K., Szweda, L. I., Chae, H. Z., and Stadtman, E. R. (1993) Immunochemical detection of 4-hydroxynonenal protein adducts in oxidized hepatocytes. *Proc. Natl. Acad. Sci. U. S. A.* **90,** 8742–8746
27. Adam, G. C., Sorensen, E. J., and Cravatt, B. F. (2002) Proteomic profiling of mechanistically distinct enzyme classes using a common chemotype. *Nat. Biotechnol.* **20,** 805–809
28. Jessani, N., Niessen, S., Wei, B. Q., Nicolau, M., Humphrey, M., Ji, Y., Han, W., Noh, D. Y., Yates, J. R., 3rd, Jeffrey, S. S., and Cravatt, B. F. (2005) A streamlined platform for high-content functional proteomics of primary human specimens. *Nat. Methods* **2,** 691–697
29. Dennehy, M. K., Richards, K. A. M., Wernke, G. W., Shyr, Y., and Liebler, D. C. (2006) Cytosolic and nuclear protein targets of thiol-reactive electrophiles. *Chem. Res. Toxicol.* **19,** 20–29
30. Greco, T. M., Hodara, R., Parastatidis, I., Heijnen, H. F., Dennehy, M. K., Liebler, D. C., and Ischiropoulos, H. (2006) Identification of S-nitrosylation motifs by site-specific mapping of the S-nitrosocysteine proteome in human vascular smooth muscle cells. *Proc. Natl. Acad. Sci. U. S. A.* **103,** 7420–7425
31. Shin, N. Y., Liu, Q., Stamer, S. L., and Liebler, D. C. (2007) Protein targets of reactive electrophiles in human liver microsomes. *Chem. Res. Toxicol.* **20,** 859–867
32. Begley, T. J., Rosenbach, A. S., Ideker, T., and Samson, L. D. (2002) Damage recovery pathways in Saccharomyces cerevisiae revealed by genomic phenotyping and interactome mapping. *Mol. Cancer Res.* **1,** 103–112
33. Said, M. R., Begley, T. J., Oppenheim, A. V., Lauffenburger, D. A., and Samson, L. D. (2004) Global network analysis of phenotypic effects: protein networks and toxicity modulation in Saccharomyces cerevisiae. *Proc. Natl. Acad. Sci. U. S. A.* **101,** 18006–18011
34. Workman, C. T., Mak, H. C., McCuine, S., Tagne, J. B., Agarwal, M., Ozier, O., Begley, T. J., Samson, L. D., and Ideker, T. (2006) A systems approach to mapping DNA damage response pathways. *Science* **312,** 1054–1059
35. Haugen, A. C., Kelley, R., Collins, J. B., Tucker, C. J., Deng, C., Afshari, C. A., Brown, J. M., Ideker, T., and Van Houten, B. (2004) Integrating phenotypic and expression profiles to map arsenic-response networks. *Genome Biol.* **5,** R95 (1–18)
36. Zhang, B., VerBerkmoes, N. C., Langston, M. A., Uberbacher, E., Hettich, R. L., and Samatova, N. F. (2006) Detecting differential and correlated protein expression in label-free shotgun proteomics. *J. Proteome Res.* **5,** 2909–2918
37. Soreghan, B. A., Yang, F., Thomas, S. N., Hsu, J., and Yang, A. J. (2003) High-throughput proteomic-based identification of oxidatively induced protein carbonylation in mouse brain. *Pharm. Res.* **20,** 1713–1720
38. Mirzaei, H., and Regnier, F. (2005) Affinity chromatographic selection of

carbonylated proteins followed by identification of oxidation sites using tandem mass spectrometry. *Anal. Chem.* **77,** 2386–2392

39. Ham, A. J. (2005) Proteolytic Digestion Protocols. In *The Encyclopedia of Mass Spectrometry: Biological Applications, Part A: Peptides and Proteins* (Caprioli, R. M., and Gross, M. L., eds) Vol. 2, pp. 10–17, Elsevier Ltd., Kidlington, Oxford, UK

40. Yates, J. R., Eng, J. K., McCormack, A. L., and Schieltz, D. (1995) Method to correlate tandem mass spectra of modified peptides to amino acid sequences in the protein database. *Anal. Chem.* **67,** 1426–1436

41. McDonald, W. H., Tabb, D. L., Sadygov, R. G., MacCoss, M. J., Venable, J., Graumann, J., Johnson, J. R., Cociorva, D., and Yates, J. R., III (2004) MS1, MS2, and SQT-three unified, compact, and easily parsed file formats for the storage of shotgun proteomic spectra and identifications. *Rapid Commun. Mass Spectrom.* **18,** 2162–2168

42. Zhang, B., Chambers, M. C., and Tabb, D. L. (2007) Proteomic parsimony through bipartite graph analysis improves accuracy and transparency. *J. Proteome Res.* **6,** 3549–3557

43. Benjamini, Y., and Hochberg, Y. (1995) Controlling the false discovery rate: a practical and powerful approach to multiple testing. *J. R. Stat. Soc. [Ser. B]* **57,** 289–300

44. Freeman, M. F., and Tukey, J. W. (1950) Transformations related to the angular and the square root. *Ann. Math. Statist.* **21,** 607–611

45. Zhang, B., Kirov, S., and Snoddy, J. (2005) WebGestalt: an integrated system for exploring gene sets in various biological contexts. *Nucleic Acids Res.* **33,** W741–W748

46. Watts, D. J., and Strogatz, S. H. (1998) Collective dynamics of 'small-world' networks. *Nature* **393,** 440–442

47. Maslov, S., and Sneppen, K. (2002) Protein interaction networks beyond artifacts. *FEBS Lett.* **530,** 255–256

48. Palla, G., Derenyi, I., Farkas, I., and Vicsek, T. (2005) Uncovering the overlapping community structure of complex networks in nature and society. *Nature* **435,** 814–818

49. Shannon, P., Markiel, A., Ozier, O., Baliga, N. S., Wang, J. T., Ramage, D., Amin, N., Schwikowski, B., and Ideker, T. (2003) Cytoscape: a software environment for integrated models of biomolecular interaction networks. *Genome Res.* **13,** 2498–2504

50. Sayre, L. M., Lin, D., Yuan, Q., Zhu, X., and Tang, X. (2006) Protein adducts generated from products of lipid oxidation: focus on HNE and one. *Drug Metab. Rev.* **38,** 651–675

51. Vila, A., Tallman, K., Jacobs, A., Liebler, D., Porter, N., and Marnett, L. (2008) Identification of protein targets of 4-hydroxynonenal using click chemistry for *ex Vivo* biotinylation of azido and alkynyl derivatives. *Chem. Res. Toxicol.* **21,** 432–444

52. West, J. D., Ji, C., Duncan, S. T., Amarnath, V., Schneider, C., Rizzo, C. J., Brash, A. R., and Marnett, L. J. (2004) Induction of apoptosis in colorectal carcinoma cells treated with 4-hydroxy-2-nonenal and structurally related aldehydic products of lipid peroxidation. *Chem. Res. Toxicol.* **17,** 453–462

53. West, J. D., and Marnett, L. J. (2005) Alterations in gene expression induced by the lipid peroxidation product, 4-hydroxy-2-nonenal. *Chem. Res. Toxicol.* **18,** 1642–1653

54. Szapacs, M. E., Riggins, J. N., Zimmerman, L. J., and Liebler, D. C. (2006) Covalent adduction of human serum albumin by 4-hydroxy-2-nonenal: kinetic analysis of competing alkylation reactions. *Biochemistry* **45,** 10521–10528

55. Liu, H., Sadygov, Rovshan G., and Yates, John R., III (2004) A model for random sampling and estimation of relative protein abundance in shotgun proteomics. *Anal. Chem.* **76,** 4193–4201

56. Saxon, E., and Bertozzi, C. R. (2000) Cell surface engineering by a modified Staudinger reaction. *Science* **287,** 2007–2010

57. Kessova, I. G., and Cederbaum, A. I. (2005) The effect of CYP2E1-dependent oxidant stress on activity of proteasomes in HepG2 cells. *J. Pharmacol. Exp. Ther.* **315,** 304–312

58. Cecarini, V., Ding, Q., and Keller, J. N. (2007) Oxidative inactivation of the proteasome in Alzheimer's disease. **41,** *Free Radic. Res.* 673–680

59. Okada, K., Wangpoengtrakul, C., Osawa, T., Toyokuni, S., Tanaka, K., and Uchida, K. (1999) 4-Hydroxy-2-nonenal-mediated impairment of intracellular proteolysis during oxidative stress. Identification of proteasomes as target molecules. *J. Biol. Chem.* **274,** 23787–23793

60. Ferrington, D. A., and Kapphahn, R. J. (2004) Catalytic site-specific inhibition of the 20 S proteasome by 4-hydroxynonenal. *FEBS Lett.* **578,** 217–223

61. Zhang, Q., Powers, E. T., Nieva, J., Huff, M. E., Dendle, M. A., Bieschke, J., Glabe, C. G., Eschenmoser, A., Wentworth, P., Jr., Lerner, R. A., and Kelly, J. W. (2004) Metabolite-initiated protein misfolding may trigger Alzheimer's disease. *Proc. Natl. Acad. Sci. U. S. A.* **101,** 4752–4757

62. Goldberg, A. L. (2003) Protein degradation and protection against misfolded or damaged proteins. *Nature* **426,** 895–899

63. Valpuesta, J. M., Martin-Benito, J., Gomez-Puertas, P., Carrascosa, J. L., and Willison, K. R. (2002) Structure and function of a protein folding machine: the eukaryotic cytosolic chaperonin CCT. *FEBS Lett.* **529,** 11–16